**10th World Congress on Structural and Multidisciplinary Optimization**
May 19 - 24, 2013, Orlando, Florida, USA

# Robust topology optimization of slender structures with geometric imperfections

**Miche Jansen[1], Geert Lombaert[1], Mattias Schevenels[2], Boyan S. Lazarov[3], Ole Sigmund[3]**

[1]Department of Civil Engineering, KU Leuven, Leuven, Belgium, miche.jansen@bwk.kuleuven.be, geert.lombaert@bwk.kuleuven.be
[2]Department of Architecture, Urbanism and Planning, KU Leuven, Leuven, Belgium, mattias.schevenels@asro.kuleuven.be
[3]Department of Mechanical Engineering, Solid Mechanics, DTU, Lyngby, Denmark, bsl@mek.dtu.dk, sigmund@mek.dtu.dk

**1. Abstract**
Structural topology optimization often leads to slender structures which are sensitive to geometric imperfections such as the misplacement of material. A robust approach is therefore presented in order to take into account material misplacement in topology optimization problems. A probabilistic approach to robust optimization is followed. Spatially varying geometric imperfections are modeled by means of a vector-valued Gaussian random field. Both a linear elastic and a nonlinear elastic formulation are considered in order to analyze the importance of geometric nonlinear effects on the design performance and the optimized design. The objective function of the robust optimization problem is defined as a weighted sum of the mean value and the standard deviation of the performance of the structure under uncertainty. A sampling method is used to estimate these statistics and the sensitivities thereof in the optimization algorithm. The solutions obtained by the robust approach are verified by means of an extensive Monte Carlo simulation.
**2. Keywords:** Topology optimization, robust design optimization, geometric imperfections, random fields

## 3. Introduction

Structural design optimization is an essential part of engineering in order to realize highly performing designs at a low cost. Topology optimization is a powerful tool in this respect as it simultaneously optimizes the size, shape and topology of a design, often resulting in new and original designs. This has led to its widespread deployment in various fields of applications.
The designs obtained by a classical deterministic optimization however are often only optimal for a single set of input data and variations in the system can drastically decrease the performance of the design or even make it infeasible. A structure is subjected to multiple sources of uncertainty: loads, material properties, manufacturing errors, environmental conditions, etc. In robust optimization [2, 5], these uncertainties are taken into account in the optimization in order to find well-performing designs which are also insensitive with respect to variations in the system.
This paper focuses on geometric imperfections as a source of uncertainty in the design of mechanical structures. In particular, we consider uncertainty in the actual location of structural elements which can deviate from the ideal nominal design. Material misplacement is encountered in civil engineering applications and originates, for example, from errors during the manufacturing process. Designs consisting of axially loaded slender elements are particularly sensitive to material misplacement due to their small stiffness for the additional bending moments which occur when the element is distorted. Moreover, the vulnerability of compressed slender members to geometric imperfections becomes especially apparent when nonlinear phenomena such as $P-\Delta$ effects and buckling are considered. A nonlinear elastic formulation is therefore adopted in this study in order to account for the geometric nonlinear behavior of the design.
A robust approach is presented which incorporates geometric imperfections due to misplacement of material into continuum topology optimization. Several paradigms to robust optimization exist in the literature [5]. This study adopts a probabilistic approach: probability distributions are attributed to the uncertainties and probabilistic moments are used to assess the robust performance of a design.
The paper starts with a brief description of topology optimization of deterministic mechanical structures. Afterwards, geometric imperfections are discussed and a random field model for spatially varying

geometric imperfections in the design domain is presented. A robust formulation of the optimization problem is applied in order to incorporate the uncertainties in the optimization problem. The presented methodology is applied in the robust design of slender column-like structures and a cantilever.

## 4. Density based topology optimization

Topology optimization of structures with linear elastic material properties is considered in this paper. The goal of topology optimization is to find the optimal distribution of material in a design domain $\Omega$ for a given set of constraints and boundary conditions. The design domain $\Omega$ is discretized by means of $n_\mathrm{e}$ finite elements in order to model the elasticity problem in the domain. The structure is parametrized by assigning a physical material density $\bar{\rho}_e$ to every element in the design domain [4]. The volume densities take values between zero and one which corresponds to the absence or presence of material, respectively. The volume fraction of the design domain occupied by the structure is therefore expressed as:

$$V = \frac{1}{V_\Omega} \sum_{e=1}^{n_\mathrm{e}} v_e \bar{\rho}_e \tag{1}$$

where $v_e$ is the volume of element $e$ and the volume of the design domain $V_\Omega = \sum_{e=1}^{n_\mathrm{e}} v_e$. The volume densities are allowed to vary between zero and one in order to obtain a smooth and differentiable optimization problem. Intermediate densities ($0 < \bar{\rho}_e < 1$), however, usually lack a physical interpretation and should be avoided in the optimized design. In the Solid Isotropic Material with Penalization (SIMP) method [3, 15], intermediate densities are therefore penalized in the stiffness interpolation:

$$E_e = E_\mathrm{min} + (E_0 - E_\mathrm{min})\, \bar{\rho}_e^p \tag{2}$$

where $E_0$ and $E_\mathrm{min}$ are the Young's moduli of the material and void phase, respectively. Intermediate densities are made inefficient by selecting the penalization parameter $p > 1$.

A density filter is commonly introduced in the design parametrization in order to avoid mesh dependence of the solution and restrict the complexity of the optimized design [6, 7]. The vector of physical densities $\bar{\boldsymbol{\rho}}$ is therefore defined as a function of a new set of design variables $\boldsymbol{\rho} \in \mathbb{R}^{n_\mathrm{e}}$. The density filter averages the design variables $\rho_e$ with a suitable low-pass filter function to obtain the intermediate densities $\tilde{\rho}_e$:

$$\tilde{\rho}_e = \frac{\sum_{i=1}^{n_\mathrm{e}} \kappa_{ei} v_i \rho_i}{\sum_{i=1}^{n_\mathrm{e}} \kappa_{ei} v_i} \tag{3}$$

The filter weights $\kappa_{ei}$ are defined as:

$$\kappa_{ei} = \max(R - \|\mathbf{x}_e - \mathbf{x}_i\|_2, 0) \tag{4}$$

where $\mathbf{x}_e$ are the coordinates of the center of element $e$ and the filter radius $R$ is related to the desired minimum length scale in the structure.

The smoothing operation (3) removes rapid variations in the design variables, but also introduces unwanted gray transition zones between material and void phase. These are removed in the following step by projecting the intermediate variables $\tilde{\rho}_e$ by means of a regularized Heaviside function [11, 18]:

$$\bar{\rho}_e = \frac{\tanh(\beta\eta) + \tanh(\beta(\tilde{\rho}_e - \eta))}{\tanh(\beta\eta) + \tanh(\beta(1 - \eta))} \tag{5}$$

where the parameter $\beta$ determines the steepness of the function and $\eta \in [0; 1]$ is the threshold value of the projection.

This study considers the minimum compliance optimization problem where the goal is to find the design which minimizes the work done by external forces for a limited amount of material:

$$\begin{aligned} \min_{\boldsymbol{\rho}} \quad & f(\boldsymbol{\rho}) = \mathbf{f}^\mathrm{T} \mathbf{u}(\boldsymbol{\rho}) \\ \text{s.t.} \quad & V(\boldsymbol{\rho}) - V_\mathrm{max} \leq 0 \\ & \mathbf{0} \leq \boldsymbol{\rho} \leq \mathbf{1} \end{aligned} \tag{6}$$

where the volume fraction $V(\boldsymbol{\rho})$ of the design is limited to a certain value $V_\mathrm{max}$. The nodal load vector $\mathbf{f}$ contains the discretized external forces. The nodal displacements $\mathbf{u}$ of the design are determined as the

solution of the finite element equilibrium equations. When small strains and displacements are assumed, this amounts to solving the following linear system:

$$\mathbf{g}_{\mathrm{l}}\left(\boldsymbol{\rho}, \mathbf{u}\right) = \mathbf{K}(\boldsymbol{\rho})\mathbf{u} - \mathbf{f} = \mathbf{0} \tag{7}$$

The linear stiffness matrix $\mathbf{K}(\boldsymbol{\rho})$ is assembled from the element stiffness matrices $\mathbf{K}_e(\boldsymbol{\rho}) = E_e(\boldsymbol{\rho})\mathbf{K}_e^0$ where $\mathbf{K}_e^0$ is the element stiffness matrix for unit-stiffness.
Slender structures are often sensitive to nonlinear phenomena such as $P-\Delta$ effects and buckling. Therefore, a large displacement formulation is also adopted in the following. When geometric nonlinearity is taken into account, the equilibrium equations are written in the general form:

$$\mathbf{g}_{\mathrm{nl}}\left(\boldsymbol{\rho}, \mathbf{u}\right) = \mathbf{r}\left(\boldsymbol{\rho}, \mathbf{u}\right) - \mathbf{f} = \mathbf{0} \tag{8}$$

The internal force vector $\mathbf{r}$ is given by the following integral over the undeformed configuration of the domain:

$$\mathbf{r}\left(\boldsymbol{\rho}, \mathbf{u}\right) = \sum_{e=1}^{n_{\mathrm{e}}} E_e(\boldsymbol{\rho}) \int_{\Omega_e} \mathbf{B}^{\mathrm{T}}(\mathbf{u})\mathbf{C}^0\mathbf{E}(\mathbf{u})\,\mathrm{d}\Omega \tag{9}$$

where $\mathbf{E}$ is the Green-Lagrange strain vector, $\mathbf{B}$ is the strain increment matrix and $\mathbf{C}^0$ the elastic constitutive matrix for unit-stiffness. The reader is referred standard textbooks [19, 20] for more detailed information on this formulation.
Equation (8) is solved by means of the Newton-Raphson method, i.e. by iteratively solving a number of local linearizations of the nonlinear system (8):

$$\mathbf{K_T}(\boldsymbol{\rho}, \mathbf{u}^{(k)})\Delta\mathbf{u}^{(k)} = -\mathbf{g}_{\mathrm{nl}}(\boldsymbol{\rho}, \mathbf{u}^{(k)}) \tag{10}$$

where $\Delta\mathbf{u}^{(k)} = \mathbf{u}^{(k+1)} - \mathbf{u}^{(k)}$ is the displacement increment and the tangent stiffness matrix $\mathbf{K_T}$ is defined as the Jacobian of $\mathbf{r}$:

$$\mathbf{K_T}(\boldsymbol{\rho}, \mathbf{u}) = \frac{\partial \mathbf{r}(\boldsymbol{\rho}, \mathbf{u})}{\partial \mathbf{u}} \tag{11}$$

In a nonlinear setting, the objective function $f = \mathbf{f}^{\mathrm{T}}\mathbf{u}$ no longer corresponds to the external work and is commonly referred to as the end-compliance [8]. In the following, nonlinear end-compliance is denoted by $f_{\mathrm{nl}}$ and linear compliance by $f_{\mathrm{l}}$.

## 5. Geometric imperfections

Two approaches are distinguished for incorporating misplacement of material in topology optimization. A perturbation of the structural members can be achieved by varying the location of the nodes in the finite element model [1, 10]. Varying the nodes can be considered as a Lagrangian approach since the computational grid (i.e. finite element mesh) follows the geometry of the design.
Alternatively, material misplacement can be modeled on a fixed Eulerian grid by modifying the mapping between the design variables $\boldsymbol{\rho}$ and $\tilde{\boldsymbol{\rho}}$ in the density filter step [12]. This approach is inspired by the variable threshold method in the projection step which is used to model variations in the cross-section of elements [16, 18]. Misplacement of material can be modeled by adding a small random perturbation vector $\mathbf{p}(\mathbf{x}_e, \theta)$ to the filter function (4) in the density filter:

$$\kappa_{ei} = \max(R - \|\mathbf{x}_e - \mathbf{p}(\mathbf{x}_e, \theta) - \mathbf{x}_i\|_2, 0) \tag{12}$$

Figure 1 illustrates the modification of the density filter in eq. (3) when the perturbed kernel in eq. (12) is used. In the nominal case (figure 1(a)) the filter kernel is centered around the centroid of the finite element and $\tilde{\rho}_e$ is determined by the element densities $\boldsymbol{\rho}$ in its neighborhood. By adding the perturbation $\mathbf{p}(\mathbf{x}_e, \theta)$, $\tilde{\rho}_e$ is determined by the densities of the neighborhood of a shifted location (figure 1(b)).
Deforming the mesh and perturbing the filter are both easy to implement and viable approaches for modeling material misplacement. Strong distortions of the mesh should be avoided in the former method however, while the latter requires modifying the boundary conditions in static mechanical problems according to the geometric imperfections.

### 5.2. Random field representation

Spatially varying geometric imperfections are modeled by means of a Gaussian random field $\mathbf{p}(\mathbf{x}, \theta)$ in

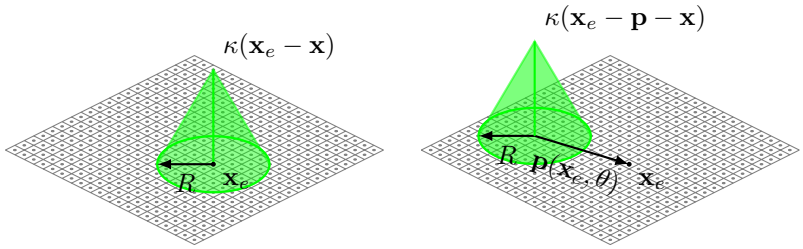


(a) Density filter (b) Perturbed density filter

Figure 1: Translation of material by a perturbation of the center of the filter kernel

the design domains. A Gaussian random field is fully characterized by its mean function $\mathbf{m}_\mathbf{p}(\mathbf{x})$ and covariance function $\mathbf{C}_\mathbf{p}(\mathbf{x}_1, \mathbf{x}_2)$:

$$\mathbf{m}_\mathbf{p}(\mathbf{x}) = \mathbb{E}\left[\mathbf{p}(\mathbf{x}, \theta)\right] \tag{13}$$

$$\begin{aligned}\mathbf{C}_\mathbf{p}(\mathbf{x}_1, \mathbf{x}_2) &= \mathrm{Cov}\left[\mathbf{p}(\mathbf{x}_1, \theta), \mathbf{p}(\mathbf{x}_2, \theta)\right] \\ &= \mathbb{E}\left[\left(\mathbf{p}(\mathbf{x}_1, \theta) - \mathbf{m}_\mathbf{p}(\mathbf{x}_1)\right)\left(\mathbf{p}(\mathbf{x}_2, \theta) - \mathbf{m}_\mathbf{p}(\mathbf{x}_2)\right)^\mathrm{T}\right]\end{aligned} \tag{14}$$

where $\mathbb{E}$ is the expectation operator. The components of the random vector $\mathbf{p}(\mathbf{x}, \theta)$ are assumed to be uncorrelated in the present study which enables the following representation of the covariance function:

$$\mathbf{C}_\mathbf{p}(\mathbf{x}_1, \mathbf{x}_2) = \begin{bmatrix} C_{\mathrm{p}_1}(\mathbf{x}_1, \mathbf{x}_2) & 0 \\ 0 & C_{\mathrm{p}_2}(\mathbf{x}_1, \mathbf{x}_2) \end{bmatrix} \tag{15}$$

A squared exponential covariance function is used for the covariance function $C_{\mathrm{p}_i}$ of component $p_i$ of the random vector:

$$C_{\mathrm{p}_i}(\mathbf{x}_1, \mathbf{x}_2) = \sigma_{\mathrm{p}_i}^2 \exp\left[-\left(\left(\frac{x_1 - x_2}{l_{cx}}\right)^2 + \left(\frac{y_1 - y_2}{l_{cy}}\right)^2\right)\right] \tag{16}$$

where $\sigma_{\mathrm{p}_i}$ is the standard deviation of the component $p_i$ of the random field and $l_{cx}$ and $l_{cy}$ are the correlation lengths of the random field in the coordinate directions $x$ and $y$.
In most cases it is necessary to assume that the structure is placed correctly on the supports – i.e. the geometric imperfections are zero at the location of the supports. Furthermore, misplacement is likely to be larger for parts of the structure which are located further from the supports. These constraints are included in the Gaussian random field by replacing the covariance function by a conditional covariance function with known values [1, 9]. The conditional covariance function $\tilde{\mathbf{C}}_\mathbf{p}(\mathbf{x}_1, \mathbf{x}_2)$ is given by the following expression when there is a set of points $\{\bar{\mathbf{x}}_i \in \Omega | i \in 1, \ldots, m\}$ where the value of the random field is fixed:

$$\begin{aligned}\tilde{\mathbf{C}}_\mathbf{p}(\mathbf{x}_1, \mathbf{x}_2) &= \mathrm{Cov}\left[\mathbf{p}(\mathbf{x}_1, \theta), \mathbf{p}(\mathbf{x}_2, \theta) | \mathbf{p}(\bar{\mathbf{x}}_i, \theta) = 0\right] \\ &= \mathbf{C}_\mathbf{p}(\mathbf{x}_1, \mathbf{x}_2) - \mathbf{C}_{\mathbf{p}\bar{\mathbf{p}}}^\mathrm{T}(\mathbf{x}_1)\mathbf{C}_{\bar{\mathbf{p}}\bar{\mathbf{p}}}^{-1}\mathbf{C}_{\mathbf{p}\bar{\mathbf{p}}}(\mathbf{x}_2)\end{aligned} \tag{17}$$

where $\mathbf{C}_{\mathbf{p}\bar{\mathbf{p}}}(\mathbf{x})$ is covariance function of $\mathbf{p}(\mathbf{x})$ and $\mathbf{p}(\bar{\mathbf{x}}_i)$ and $\mathbf{C}_{\bar{\mathbf{p}}\bar{\mathbf{p}}}$ is the covariance matrix of $\mathbf{p}(\bar{\mathbf{x}}_i)$.
A discrete approximation of the Gaussian random field $\mathbf{p}(\mathbf{x}, \theta)$ is established by means of the Expansion Optimal Linear Estimation method (EOLE) by Li and Der Kiureghian [14]. In the EOLE method, the random field is initially only considered in a discrete number of points $N$ in the domain $\Omega$. The random vector corresponding to the values of the random field in these points is a multivariate normally distributed random vector which is decorrelated by means of principal component analysis. At intermediate locations, the random field is approximated by means of the Optimal Linear Estimator (OLE) method. The resulting EOLE expansion is written as a sum of deterministic mode functions $\boldsymbol{\varphi}_i$ multiplied by standard normal random variables $\xi_i(\theta)$:

$$\mathbf{p}(\mathbf{x}, \theta) \approx \sum_{i=1}^{M} \boldsymbol{\varphi}_i(\mathbf{x})\xi_i(\theta) \tag{18}$$

where $M \leq N$ is the number of modes included in the expansion.

## 6. Robust optimization

When the random field model for imperfections is introduced in the structure, the uncertain performance $f(\boldsymbol{\rho}, \boldsymbol{\xi})$ depends on the design variables $\boldsymbol{\rho}$ and the random variables $\boldsymbol{\xi}$. The uncertainties are taken into account in the robust optimization problem by defining the objective function as a weighted sum of the mean and standard deviation of the performance:

$$\begin{aligned} \min_{\boldsymbol{\rho}} \; & m_f(\boldsymbol{\rho}) + \omega \sigma_f(\boldsymbol{\rho}) \\ \text{s.t. } & V(\boldsymbol{\rho}) - V_{\max} \leq 0 \\ & \mathbf{0} \leq \boldsymbol{\rho} \leq \mathbf{1} \end{aligned} \tag{19}$$

where the weighting parameter $\omega$ is chosen equal to 1 in this study. The mean $m_f$ and standard deviation $\sigma_f$ of the objective function are defined as:

$$m_f(\boldsymbol{\rho}) = \mathbb{E}\left[f(\boldsymbol{\rho}, \boldsymbol{\xi})\right] \tag{20}$$

$$\sigma_f(\boldsymbol{\rho}) = \sqrt{\mathbb{E}\left[\left(f(\boldsymbol{\rho}, \boldsymbol{\xi})\right)^2 - \left(m_f(\boldsymbol{\rho})\right)^2\right]} \tag{21}$$

The robust optimization problem is solved by estimating the stochastic moments $m_f$ and $\sigma_f$ and the design sensitivities of these quantities once in every iteration step of the optimization algorithm. A numerical integration rule is used to approximate the expectation operator by a weighted sum:

$$\mathbb{E}[f(\boldsymbol{\rho}, \boldsymbol{\xi})] \approx \sum_{i=1}^{q} w_i f(\boldsymbol{\rho}, \boldsymbol{\xi}_i) \tag{22}$$

where $q$ is the number of sampling points $\boldsymbol{\xi}_i$ used and $w_i$ are the integration weights. Some integration rules applicable to (22) are the Monte Carlo method, Gaussian quadrature, sparse grid quadrature or Quasi-Monte Carlo [13].

## 7. Examples

The presented robust approach is applied in three structural design problems. The topology optimization problems are solved numerically by means of the method of moving asymptotes (MMA) [17]. The following material properties are used in the SIMP law (2) throughout the examples: a penalization parameter $p = 3$ and Young's moduli $E_0 = 200$ GPa and $E_{\min} = 10^{-9} E_0$.

### 7.1. Clamped column design

The design of a slender column-like structure is considered in this example. The design domain and boundary conditions for the topology optimization problem are shown in figure 2(a). The design domain with a height $H = 3$ m and an out-of-plane thickness $t = 0.01$ m is discretized with $288 \times 96$ square plane elements. A distributed load with a width of $H/12$ is applied at the top edge. The integrated total load is equal to $P = 428$ kN. The bottom edge of the design domain is clamped. The maximum allowed volume fraction is equal to $V_{\max} = 0.25$. The density filter uses a filter radius $R = 0.0215H$, a projection threshold $\eta = 0.5$ and a maximum value for the steepness $\beta = 32$.

The analysis is first restricted to small linear displacements. As expected, the nominal optimal design (figure 2(b)) is a straight column which transfers the load directly to the foundation.

Only horizontal imperfections are considered as perturbations of the column. The corresponding random field is described by the following parameters: $\sigma_{\mathrm{p}_x} = 0.0208H$, $\sigma_{\mathrm{p}_y} = 0$, $l_{cx} = \infty$ and $l_{cy} = H$. Furthermore, the random field is conditioned such that the geometric imperfections are zero at the clamped base at the bottom of the domain. The random field is discretized using the EOLE method with 6 points equally distributed along the height of the domain domain. The six EOLE modes $\varphi_i(\mathbf{x})$ are illustrated in figure 3 by applying them to the nominal optimal design. Only the first three modes are included in the EOLE expansion as the mean square error after truncation already approaches zero for this number [12].

Tensorized Gaussian quadrature is used to estimate the mean and standard deviation of the compliance in the robust optimization. A 3-point rule is used in every dimension which leads to a total of $q = 27$ quadrature points. The robust design is shown in figure 2(c). The design contains two separate legs in order to increase its robustness with respect to misplacement. The two legs of the structure are connected by a thinner cross-bracing which increases the stability of the two separate legs. The results

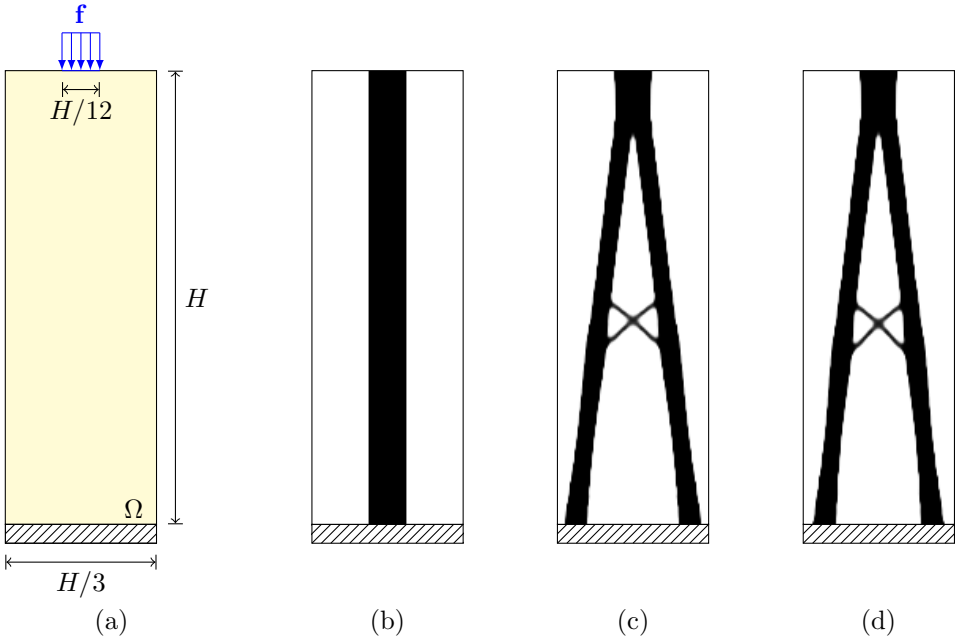


Figure 2: Clamped column: (a) design domain and boundary conditions, (b) nominal design, (c) linear robust design and (d) nonlinear robust design.

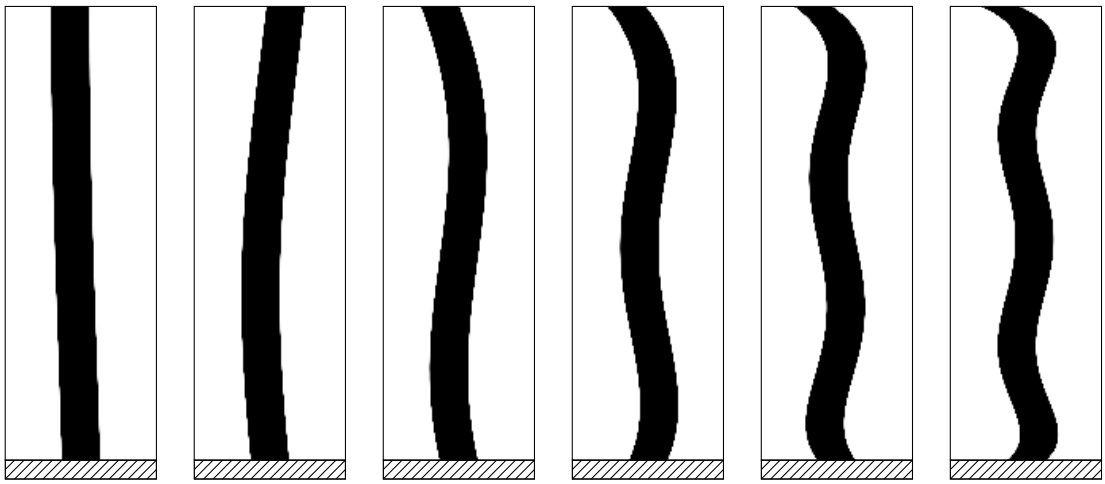


Figure 3: Modes of the EOLE expansion of the Gaussian random field $\mathbf{p}(\mathbf{x}, \theta)$ applied to the nominal column design. The modes $\varphi(\mathbf{x})$ are normalized and multiplied by a constant factor = 80 in order to show the difference in mode shape.

for the designs are compared in table 1. As expected, the nominal performance of the robust design is slightly worse than for the nominal design. The robust design however is less sensitive to imperfections as indicated by the significantly smaller mean $m_{f_1}$ and standard deviation $\sigma_{f_1}$ of the performance.
The sensitivity of the nominal design to geometric imperfections becomes even more apparent when geometric nonlinear behavior is considered. The magnitude of the load is currently at approximately 60 % of the theoretical Euler buckling load $P_1 = 714$ kN of the nominal design. The statistics of the nonlinear end-compliance are shown in the last two columns of table 1: there is a strong increase in the statistics of the nominal design. The robust design does not show any significant geometric nonlinear behavior as the nonlinear statistics are almost equal to the linear statistics.

Table 1: Results for the optimized clamped column designs: the nominal linear performance $f_{\mathrm{l}}$, the mean $m_{f_{\mathrm{l}}}$ and standard deviation $\sigma_{f_{\mathrm{l}}}$ of the linear compliance obtained by a Monte Carlo simulation with 10 000 samples, the estimated statistics at the end of the robust optimization $\hat{m}_f$ and $\hat{\sigma}_f$ and the mean $m_{f_{\mathrm{nl}}}$ and standard deviation $\sigma_{f_{\mathrm{nl}}}$ of the nonlinear end-compliance. All results are in kNm.

| Design | $f_{\mathrm{l}}$ | $m_{f_{\mathrm{l}}}$ | $\sigma_{f_{\mathrm{l}}}$ | $m_{f_{\mathrm{l}}}+\sigma_{f_{\mathrm{l}}}$ | $\hat{m}_f$ | $\hat{\sigma}_f$ | $m_{f_{\mathrm{nl}}}$ | $\sigma_{f_{\mathrm{nl}}}$ | $m_{f_{\mathrm{nl}}}+\sigma_{f_{\mathrm{nl}}}$ |
|---|---|---|---|---|---|---|---|---|---|
| Nominal | 1.10 | 1.40 | 0.38 | 1.77 | / | / | 2.42 | 1.83 | 4.25 |
| Linear robust | 1.21 | 1.26 | 0.06 | 1.32 | 1.26 | 0.05 | 1.27 | 0.07 | 1.34 |
| Nonlinear robust | 1.21 | 1.26 | 0.05 | 1.31 | 1.27 | 0.06 | 1.27 | 0.06 | 1.33 |

Figure 4 shows the compliance of the nominal and robust design as a function of the first imperfection mode $\varphi_1(\mathbf{x})$. The nonlinear end-compliance is shown for different load levels $\lambda = P/P_1$ and normalized by $f_N = f_{\mathrm{nl}}/\lambda^2$ in order to illustrate the increasing influence of geometric nonlinear effects for larger loads.
It should be noted that including geometric nonlinearity in the present optimization problem does not lead to a significant difference in design. Clearly, the straight column remains the optimal nominal design, surely when the load remains below its first buckling load. Furthermore, the nonlinear robust design (figure 2(d)) is almost identical to its linear counterpart.

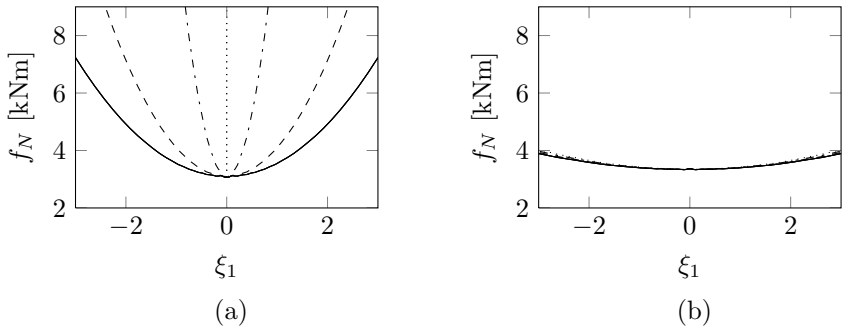


Figure 4: Clamped column: performance as a function of the first mode of imperfection for (a) the nominal design and (b) the robust design: normalized linear compliance (full line) and nonlinear end-compliance for load levels $\lambda = 40$ % (dashed line), $\lambda = 80$ % (dash-dotted line) and $\lambda = 120$ % (dotted line).

7.2. Cantilever structure

The second example considers the optimization of a cantilever design. Figure 5(a) shows the design domain and boundary conditions. The design domain $\Omega$ has a height $H = 1$ m, a length $L = 2.4$ m and out-of-plane thickness $t = 0.01$ m. A point load $P = 1111$ kN is applied a distance $d = 0.12$ m from the upper and right edge of the design domain. The maximum volume fraction is $V_{\max} = 1/4$ of the design domain volume. The filter parameters are $R = 0.047$ m, a projection threshold $\eta = 0.5$ and a maximum value for the steepness $\beta = 32$.
Geometric imperfections are modeled by a random field $\mathbf{p}(\mathbf{x}, \theta)$ with $\sigma_{\mathrm{p}_1} = \sigma_{\mathrm{p}_2} = 0.04$ m and a correlation length $l_{\mathrm{c}} = 1.2$ m in both directions. The random field is conditioned such that the imperfections are zero at the clamped edge of the design domain and 20 modes are included in the EOLE expansion. The Monte Carlo method with 100 samples is used as integration rule in the robust optimization in order to easily manage the high dimensionality of the random space.
The optimized designs are shown in figure 5(b-e) and the corresponding results are given in table 2. The linear designs are considered first. Compared to the nominal design (b), two additional thin bars appear in the robust design (c). As illustrated in the paper [12], these thin bars have a stiffening effect on the diagonal bar in the middle when imperfections are present. As a results, the linear statistics for the robust design are slightly better than for the nominal design.
Next, the nonlinear designs are considered. The nominal design (d) is very similar to the linear nominal

design (b) since the applied load is relatively low. However, the robust design (e) strongly differs from the linear robust design (c). The additional thin bars do not appear in the nonlinear robust design since they are used to support bars which work in tension and therefore do not actually require any stabilization. Furthermore, the additional thin bars in the linear robust design are under compression themselves which are therefore very sensitive to material misplacement. As a result, the linear robust design has actually the worst robust performance when geometric nonlinearity is included (cf. table 2). On the other hand, the nonlinear robust design uses more material to stabilize the bars in compression, i.e. by slightly increasing the section of the lower bars. As a result, the nonlinear robust performance is significantly improved.

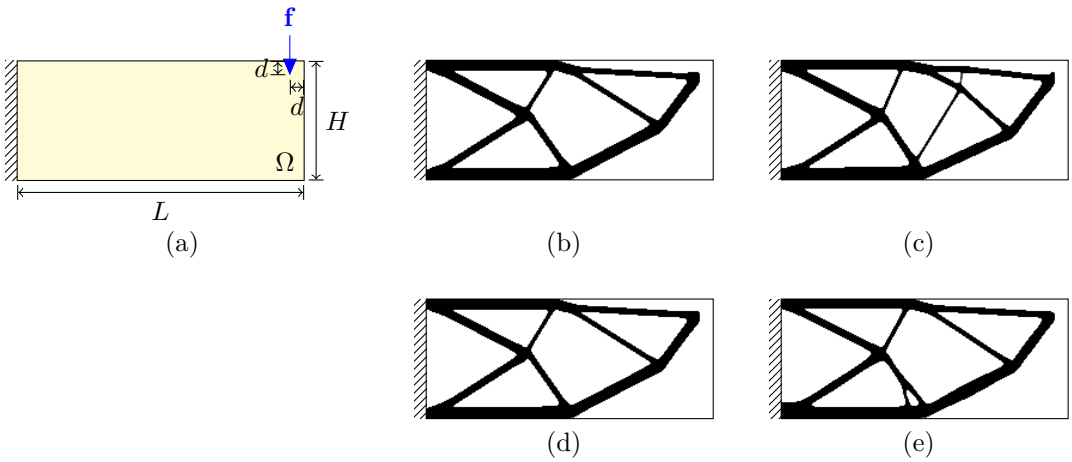


Figure 5: Cantilever design: (a) design domain and boundary conditions, (b) linear nominal design, (c) linear robust design, (d) nonlinear nominal design and (e) nonlinear robust design.

Table 2: Results for the optimized cantilever designs: the nominal linear performance $f_{\text{l}}$, the mean $m_{f_{\text{l}}}$ and standard deviation $\sigma_{f_{\text{l}}}$ of the linear compliance obtained by a Monte Carlo simulation with 10 000 samples, the estimated statistics at the end of the robust optimization $\hat{m}_f$ and $\hat{\sigma}_f$ and the mean $m_{f_{\text{nl}}}$ and standard deviation $\sigma_{f_{\text{nl}}}$ of the nonlinear end-compliance. All results are in kNm.

| Design | $f_{\text{l}}$ | $m_{f_{\text{l}}}$ | $\sigma_{f_{\text{l}}}$ | $m_{f_{\text{l}}} + \sigma_{f_{\text{l}}}$ | $\hat{m}_f$ | $\hat{\sigma}_f$ | $m_{f_{\text{nl}}}$ | $\sigma_{f_{\text{nl}}}$ | $m_{f_{\text{nl}}} + \sigma_{f_{\text{nl}}}$ |
|---|---|---|---|---|---|---|---|---|---|
| Linear nominal | 93.14 | 97.24 | 6.22 | 103.46 | / | / | 102.01 | 13.04 | 115.05 |
| Linear robust | 93.91 | 96.80 | 5.36 | 102.15 | 96.62 | 5.36 | 108.02 | 10.94 | 118.96 |
| Nonlinear nominal | 93.20 | 97.09 | 6.13 | 103.22 | / | / | 101.79 | 11.76 | 113.55 |
| Nonlinear robust | 94.57 | 98.65 | 6.36 | 105.01 | 98.62 | 6.01 | 99.12 | 6.14 | 105.26 |

## 8. Conclusions

This paper presents a method for incorporating geometric imperfections due to misplacement of material in density based topology optimization. Geometric imperfections can deteriorate the performance of slender structures such as columns and braced frames which are often encountered in civil and mechanical applications.

A probabilistic approach to robust optimization is followed and spatially varying geometric imperfections are modeled by means of a vector-valued random field in the design domain. The uncertainties are propagated in the robust optimization problem by defining the objective function as a weighted sum of the mean and standard deviation of the structural performance subjected to geometric imperfections. A nonlinear elastic formulation is adopted in order to account for the interaction between geometric imperfections and geometric nonlinear behavior in slender structures.

Two minimum compliance problems were considered in the examples. Although the robust designs typically have a slightly worse nominal performance compared to their nominal counterpart, they are less sensitive with respect to geometric imperfections as shown by the results of the extensive Monte Carlo

simulation.

**9. Acknowledgements**
The research presented in this paper has been performed within the framework of the KU Leuven - BOF PFV/10/002 OPTEC - Optimization in Engineering Center and the NextTop project sponsored by the Villum Foundation.

**10. References**

[1] M. Baitsch and D. Hartmann. Optimization of slender structures considering geometrical imperfections. *Inverse Problems in Science and Engineering*, 14(6):623–637, 2006.

[2] A. Ben-Tal, L. El Ghaoui, and A.S. Nemirovski. *Robust optimization*. Princeton Series in Applied Mathematics. Princeton University Press, 2009.

[3] M.P. Bendsøe. Optimal shape design as a material distribution problem. *Structural and Multidisciplinary Optimization*, 1:193–202, 1989.

[4] M.P. Bendsøe and O. Sigmund. *Topology optimization: Theory, Methods and Applications*. Springer, Berlin, second edition, 2004.

[5] H.G. Beyer and B. Sendhoff. Robust optimization – A comprehensive survey. *Computer Methods in Applied Mechanics and Engineering*, 196(33–34):3190–3218, 2007.

[6] B. Bourdin. Filters in topology optimization. *International Journal for Numerical Methods in Engineering*, 50(9):2143–2158, 2001.

[7] T.E. Bruns and D.A. Tortorelli. Topology optimization of non-linear elastic structures and compliant mechanisms. *Computer Methods in Applied Mechanics and Engineering*, 190(26–27):3443–3459, 2001.

[8] T. Buhl, C.B.W. Pedersen, and O. Sigmund. Stiffness design of geometrically nonlinear structures using topology optimization. *Structural and Multidisciplinary Optimization*, 19:93–104, 2000.

[9] O. Ditlevsen. Dimension reduction and discretization in stochastic problems by regression method. In F. Casciati and J.B. Roberts, editors, *Mathematical Models for Structural Reliability Analysis*, pages 51–138, 1996.

[10] J.K. Guest and T. Igusa. Structural optimization under uncertain loads and nodal locations. *Computer Methods in Applied Mechanics and Engineering*, 198(1):116–124, 2008.

[11] J.K. Guest, J.H. Prevost, and T. Belytschko. Achieving minimum length scale in topology optimization using nodal design variables and projection functions. *International Journal for Numerical Methods in Engineering*, 61(2):238–254, 2004.

[12] M. Jansen, G. Lombaert, M. Diehl, B.S. Lazarov, O. Sigmund, and M. Schevenels. Robust topology optimization accounting for misplacement of material. *Structural and Multidisciplinary Optimization*, 47:317–333, 2013.

[13] O.P. Le Maître and O.M. Knio. *Spectral Methods for Uncertainty Quantification: With Applications to Computational Fluid Dynamics*. Scientific Computation. Springer, 2010.

[14] C.C. Li and A. Der Kiureghian. Optimal discretization of random fields. *Journal of Engineering Mechanics*, 119(6):1136–1154, 1993.

[15] G.I.N. Rozvany, M. Zhou, and T. Birker. Generalized shape optimization without homogenization. *Structural and Multidisciplinary Optimization*, 4:250–252, 1992.

[16] M. Schevenels, B.S. Lazarov, and O. Sigmund. Robust topology optimization accounting for spatially varying manufacturing errors. *Computer Methods in Applied Mechanics and Engineering*, 200(49-52):3613–3627, 2011.

[17] K. Svanberg. The method of moving asymptotes – A new method for structural optimization. *International Journal for Numerical Methods in Engineering*, 24:359–373, 1987.

[18] F. Wang, B.S. Lazarov, and O. Sigmund. On projection methods, convergence and robust formulations in topology optimization. *Structural and Multidisciplinary Optimization*, 43:767–784, 2011.

[19] P. Wriggers. *Nonlinear Finite Element Methods*. Springer-Verlag Berlin Heidelberg, 2008.

[20] O.C. Zienkiewicz and R.L. Taylor. *The finite element method, Volume 2: solid mechanics*. Butterworth-Heinemann, Oxford, United Kingdom, fifth edition, 2000.